

Electronic Structure and Reactivity of Isomeric Oxo-Mn(V) Porphyrins: Effects of Spin-State Crossing and pK_a Modulation

Filippo De Angelis,^{*,†,‡} Ning Jin,[‡] Roberto Car,[‡] and John T. Groves^{*,‡}

Istituto CNR di Scienze e Tecnologie Molecolari (ISTM), c/o Dipartimento di Chimica, ISTM-CNR Perugia, Via elce di Sotto 8, I-06213, Perugia, Italy, and Department of Chemistry, Princeton University, Princeton, New Jersey 08544

Received February 22, 2006

The reactivity of the isomeric oxo-Mn(V)-2-tetra-*N*-methylpyridyl (2-TMPyP) and oxo-Mn(V)-4-tetra-*N*-methylpyridyl (4-TMPyP) porphyrins has been investigated by a combined experimental and theoretical approach based on density functional theory. The unusual higher reactivity of the more electron-rich 4-TMPyP species appears to be related to both the higher basicity of its oxo ligand, compared to that of the 2-TMPyP isomer, and the smaller low-spin–high-spin promotion energy of 4-TMPyP, compared to that of 2-TMPyP, because of the stabilization of the A_{2u} orbital in the latter isomer. Therefore, in a two-state energy profile involving crossing of the initial singlet and final quintet potential energy surfaces, the 4-TMPyP isomer should be kinetically favored. The calculated differences in the singlet–quintet gaps for the 2-TMPyP and 4-TMPyP systems compare well with the measured differences in the activation energies for two isomeric porphyrins. Both effects, proton affinity and electron-promotion energy, contribute to reduce the reactivity of the more electrophilic oxidant when electron-withdrawing groups are closer to the active site, contrary to the usual expectations based on simple chemical reactivity correlations. These theoretical results are in accord with new experimental data showing $O=Mn(V)-O-H$ pK_a s of 7.5 and 8.6 for the isomeric 2-TMPyP and 4-TMPyP systems, respectively.

Introduction

The generation of reactive oxo-transition metal species is central to the redox biochemistry of dioxygen and to a variety of catalytic processes. High-valent oxoiron porphyrins are involved in the substrate oxygenation reactions of cytochrome P450 and in the halide oxygenations typical of chloroperoxidase and myeloperoxidase.^{1,2} Reactive oxomanganese complexes are thought to participate in the photo-synthetic oxidation of water to produce oxygen.^{3–7} Synthetic,

biomimetic systems using manganese porphyrins^{8–10} and related Schiff base complexes^{11,12} have been shown to be efficient catalysts for the hydroxylation and epoxidation of a wide range of organic substrates. An important goal in the study of such metal-mediated oxidative catalysis is to gain a fuller understanding of the relationships between the reactivity and electronic structure of the metal species involved. The transient nature of these reactive intermediates, especially uncertainties regarding the electronic configurations and even ligation geometries, has been a barrier to

* To whom correspondence should be addressed. E-Mail: filippo@thch.unipg.it (F.D.A.); jtgro@princeton.edu (J.T.G.).

† ISTM-CNR Perugia.

‡ Princeton University.

- (1) (a) Groves, J. T. In *Cytochrome P450: Structure, Mechanism, and Biochemistry*, 3rd ed.; Ortiz de Montellano, P. R., Ed.; Kluwer Academic, Plenum Publishers: New York, 2005; pp 1–44. (b) Groves, J. T. *Proc. Nat. Acad. Sci.* **2003**, *100*, 3569–3574.
- (2) Meunier, B.; de Visser, S. P.; Shaik, S. *Chem. Rev.* **2004**, *104*, 3947–3980.
- (3) Carrell, T. G.; Tyryshkin, A. M.; Dismukes, G. C. *J. Biol. Inorg. Chem.* **2002**, *7*, 2–22.
- (4) Zouni, A.; Witt, H. T.; Kern, J.; Fromme, P.; Krauss, N.; Saenger, W.; Orth, P. *Nature* **2001**, *409*, 739–743.
- (5) Nugent, J. H. A.; Rich, A. M.; Evans, M. C. W. *Biochim. Biophys. Acta* **2001**, *1503*, 138–146.

- (6) Shimazaki, Y.; Nagano, T.; Takesue, H.; Ye, B. H.; Tani, F.; Naruta, Y. *Angew. Chem., Int. Ed.* **2004**, *43*, 98–100.
- (7) Shimazaki, Y.; Nagano, T.; Takesue, H.; Ye, B. H.; Tani, F.; Naruta, Y. *Angew. Chem., Int. Ed.* **2004**, *43*, 98–100.
- (8) (a) Groves, J. T.; Stern, M. K. *J. Am. Chem. Soc.* **1988**, *110*, 8628–8638. (b) Groves, J. T.; Kruper, W. J.; Haushalter, R. C. *J. Am. Chem. Soc.* **1980**, *102*, 6377–6380.
- (9) Meunier, B.; Bernadou, J. *Top. Catal.* **2002**, *21*, 47–54.
- (10) Bernadou, J.; Fabiano, A.-S.; Robert, A.; Meunier, B. *J. Am. Chem. Soc.* **1994**, *116*, 9375–9376.
- (11) Jacobsen, E. N. In *Comprehensive Organometallic Chemistry II*; Wilkinson, G. S.; Abel, E. W.; Hegedus, L. S., Eds.; Pergamon: New York, 1995; Vol. 12.
- (12) Bryliakov, K. P.; Kholdeeva, O. A.; Vanina, M. P.; Talsi, E. P. *J. Mol. Catal. A* **2002**, *178*, 47–53.

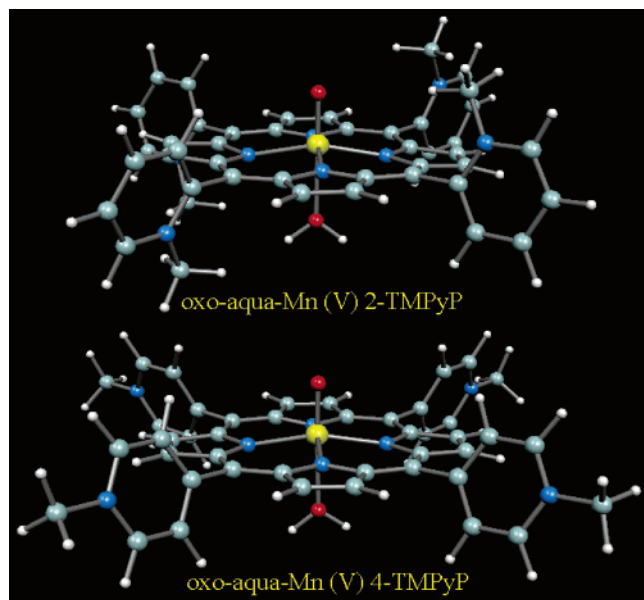


Figure 1. Optimized molecular structures of the isomeric oxo-aqua-Mn(V)-2-tetra-*N*-methylpyridyl porphyrin (oxo-Mn(V)-2-TMPyP) and oxo-aqua-Mn(V)-4-tetra-*N*-methylpyridyl porphyrin (oxo-Mn(V)-4-TMPyP) species **3**. Both species have +5 charges.

progress. In recent years, fast kinetic probes of the reactivity of oxometalloporphyrin complexes^{13,14} and the emerging power of chemical computation in such systems^{15–25} have begun to provide a new level of understanding of the nature and reactivity of such oxometal species.

We have previously shown that reactive oxomanganese(V) porphyrin complexes can be generated at ambient temperature in water.^{13,26} These species unambiguously adopt a singlet d^2 ground state, as revealed by a well-resolved proton NMR spectrum typical of a diamagnetic porphyrin.²⁶ The isomeric 2- and 4-tetra-*N*-methylpyridyl porphyrins, oxo-Mn(V)-2-TMPyP and oxo-Mn(V)-4-TMPyP, Figure 1, showed

a highly unusual reactivity pattern for both electron transfer and atom transfer reactions, with the more highly electron-deficient oxo-Mn(V)-2-TMPyP isomer reacting 1000-fold more slowly than oxo-Mn(V)-4-TMPyP. We suggested that the enhanced stability of oxo-Mn(V)-2-TMPyP with respect to its 4-pyridyl isomer was the result of a spin-state crossing effect, wherein the more electron deficient 2-pyridyl isomer has, as a result, a larger low-spin–high-spin splitting.²⁶ Thus, a singlet oxomanganese(V) complex would be obliged to promote an electron from the in-plane d_{xy} orbital to a π -antibonding $d_{xz,yz}$ orbital upon reduction. No such effects were observed for the corresponding Mn(IV) and Mn(III) complexes that have high-spin ground states. The discovery that the reaction of bromide ions with these oxo-Mn(V) porphyrins was fast and reversible and the experimental determination of both the equilibrium constant and proton dependence for this process²⁷ have provided a unique opportunity to examine this oxygen atom transfer reaction with computational methods in an effort to provide a rationale for the unusual reactivity pattern exhibited by these isomeric oxo-Mn(V) porphyrins.

We describe here the results of density functional theory (DFT) calculations for this family of spectroscopically and kinetically characterized oxo-Mn(V) porphyrin complexes. In particular, we consider the 2-TMPyP and 4-TMPyP isomers of the dioxo (**1**), oxo-hydroxo (**2**), and oxo-aqua (**3**) Mn(V) derivatives. We compute the relevant singlet (S), triplet (T), and quintet (Q) spin states for all the complexes, with the exception of the 4-TMPyP isomer where we limit the calculation of the T and Q states to the reactive oxo-aqua species **3** only. Moreover, we performed additional calculations on the two isomers of complex **3**, explicitly including 4 water molecules in the active site region, to provide a rough representation of the first solvation shell surrounding the Mn atom and the axial ligands. In all cases, we fully relax the molecular geometries using the Car–Parrinello method.²⁸ In addition, we investigate the relative energies of the S, T, and Q spin states for the di-aqua-Mn(III)-2-TMPyP species, which is the end product of the oxo-transfer process.

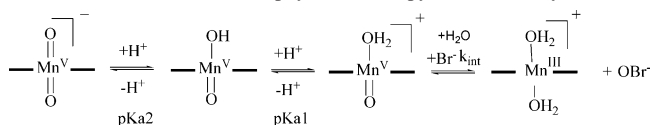
The results correctly predict the unusual reactivity pattern of these oxo-Mn(V) porphyrins with substrates. We find that the experimental results derive from two main effects. One is the spin-state effect suggested earlier,²⁶ while the other is a significant and unanticipated modulation of the pK_a of manganese-bound water, which is consistent with experimental measurements of these acidities.

Below we discuss the computational methodology, analyze the experimental data for the rate constants for the haloperoxidase-like reaction of oxo-Mn(V) porphyrins with the bromide ion to form hypobromite (BrO^-) as a function of pH, and report the calculated electronic structures and spin-state crossing effects. We conclude with a description of the electronic nature of this oxo-transfer process.

- (13) Groves, J. T.; Lee, J.; Marla, S. S. *J. Am. Chem. Soc.* **1997**, *119*, 6269–6273.
- (14) Lee, J.; Hunt, J. A.; Groves, J. T. *J. Am. Chem. Soc.* **1998**, *120*, 6053–6061.
- (15) de Visser, S. P.; Ogliaro, F.; Gross, Z.; Shaik, S. *Chem.–Eur. J.* **2001**, *7*, 4954–4960.
- (16) Ogliaro, F.; de Visser, S. P.; Groves, J. T.; Shaik, S. *Angew. Chem., Int. Ed.* **2001**, *40*, 2874–2878.
- (17) Schoneboom, J. C.; Cohen, S.; Lin, H.; Shaik, S.; Thiel, W. *J. Am. Chem. Soc.* **2004**, *126*, 4017–4034.
- (18) Shaik, S.; Cohen, S.; de Visser, S. P.; Sharma, P. K.; Kumar, D.; Kozuch, S.; Ogliaro, F.; Danovich, D. *Eur. J. Inorg. Chem.* **2004**, 207–226.
- (19) Kamachi, T.; Yoshizawa, K. *J. Am. Chem. Soc.* **2003**, *125*, 4652–4661.
- (20) Kamachi, T.; Shiota, Y.; Ohta, T.; Yoshizawa, K. *Bull. Chem. Soc. Jpn.* **2003**, *76*, 721–732.
- (21) Guallar, V.; Baik, M.-H.; Lippard, S. J.; Friesner, R. A. *Proc. Nat. Acad. Sci.* **2003**, *100*, 6998–7002.
- (22) Giannozzi, P.; De Angelis, F.; Car, R. *J. Chem. Phys.* **2004**, *120*, 5903–5915. The CP parallel code is available as part of the quantum espresso release at <http://www.quantum-espresso.org>.
- (23) Arnaud, P.; Zakrzewska, K.; Meunier, B. *J. Comput. Chem.* **2003**, *24*, 797–805.
- (24) (a) Ghosh, A.; Gonzalez, E. *Isr. J. Chem.* **2000**, *40*, 1. (b) Ghosh, A.; Vangberg, T.; Gonzalez, E.; Taylor, P. *J. Porphyrins Phthalocyanines* **2001**, *5*, 345. (c) Ghosh, A.; Taylor, P. R. *Curr. Opin. Chem. Biol.* **2003**, *7*, 113–124.
- (25) de Visser, S. P.; Kumar, D.; Neumann, R.; Shaik, S. *Angew. Chem., Int. Ed.* **2004**, *43*, 5661–5665.
- (26) Jin, N.; Groves, J. T. *J. Am. Chem. Soc.* **1999**, *121*, 2923–2924.

(27) Jin, N.; Bourassa, J. L.; Tizio, S. C.; Groves, J. T. *Angew. Chem.* **2000**, *39*, 3849–3851.

(28) Car, R.; Parrinello, M. *Phys. Rev. Lett.* **1985**, *55*, 2471.

Scheme 1. Oxo-Mn(V) Porphyrin Prototropy and Reactivity^a

^a The reported charges refer to formal oxidation states of the metal and axial ligands.

Computational Method

We use the Car–Parrinello²⁸ (CP) first-principles molecular dynamics scheme for electronic-structure calculations and structural optimizations. In this approach, the valence electronic wave functions are expanded in plane waves, and pseudopotentials are used to model the interaction of the valence electrons with the ionic cores. We use the parallel version²² of the CP code implementing Vanderbilt ultra-soft pseudopotentials.^{29,30} A cutoff of 25 Ry for the electronic orbitals and of 200 Ry for the augmented charge is sufficient for a good convergence of the structural and energetic properties. The plane wave expansion requires periodic boundary conditions. Molecular calculations are performed by placing the molecular systems in a periodically repeated cubic box. For the systems of interest here, a box side of 19.04 Å gives a minimum distance of 6.0 Å between the replicas, enough to avoid spurious overlaps between electronic orbitals belonging to different periodic images. Even in the absence of direct overlap between the wave functions, long-range electrostatic interactions between the images are present. These effects are nonnegligible particularly when the molecular systems are charged, as is the case in the present study. We eliminate the long-range electrostatic interactions among the periodic replicas using a procedure described by Makov and Payne,³¹ which accounts for monopole, dipole, and quadrupole interactions. The resulting energies are very accurate as we could check by comparing the energy difference between the different charge states of the molecules of interest in this paper with the corresponding results obtained with localized basis functions.²² We use the generalized gradient approximation (GGA) for the exchange and correlation (XC) energy within DFT. We adopt the Perdew–Wang³² form of GGA, in which gradient corrections are added to a local density approximated functional using the Perdew–Zunger³³ parametrization. Geometry optimizations are performed without any symmetry constraints by means of damped molecular dynamics.

Experimental Data and Phenomenology

The generation and reactions of oxo-Mn(V) porphyrins in aqueous solution under different pH conditions were performed as we have previously described.^{13,14,26,27} The pertinent acid–base equilibria for the reaction of interest are illustrated in Scheme 1.

The apparent second-order rate constant (k_{app}) for direct oxo transfer from manganese to the bromide ion is extracted from the data as previously described.²⁷ In Figure 2, we report k_{app} over the range of pH 9–5, for isomeric oxo-Mn(V)-2-TMPyP and oxo-Mn(V)-4-TMPyP porphyrins. This figure compares data previously obtained for 2-TMPyP with new

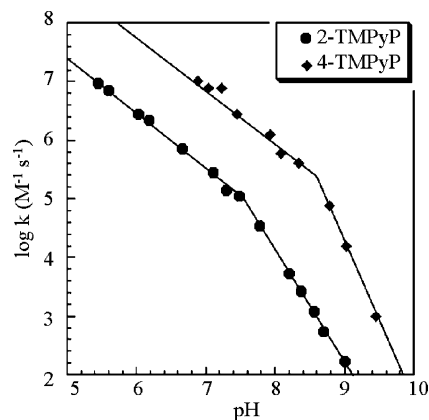


Figure 2. Log k ($\text{M}^{-1} \text{s}^{-1}$) vs pH for the isomeric oxo-Mn(V)-2-TMPyP and oxo-Mn(V)-4-TMPyP complexes.

data for 4-TMPyP obtained in the context of the present investigation. It is evident that the 4-TMPyP isomer is more reactive than 2-TMPyP toward bromide ion over the accessible pH range.³⁴ In particular, the reactivity of the 4-pyridyl isomer is approximately 2 orders of magnitude higher than the corresponding reactivity of the 2-pyridyl isomer over the entire pH range. This difference in the rate constants translates into a difference in the activation energies of ca. 3 kcal mol⁻¹ between the two isomers. The change in slope of k_{app} versus pH from one to nearly two occurring at about pH 7.5 (pH 8.6) for the 2-TMPyP (4-TMPyP) isomer defines pK_{a2} (i.e., the pK_a for the prototropic equilibrium between species 1 and 2 in Scheme 1). The change in slope occurs because species 1 has to acquire two protons to transform into the reactive species 3, whereas only one proton is needed to transform species 2 into species 3. Eventually, the rate constant should saturate at pH values sufficiently low that only species 3 would be present at equilibrium. The onset of this regime is signaled by pK_{a1} , the pK_a value corresponding to equilibrium between species 2 and 3. This value is outside the experimentally accessible pH range in Figure 2. The higher reactivity of 4-TMPyP compared to 2-TMPyP may be the result of higher intrinsic reactivity ($\Delta k_{\text{int}} > 0$), higher proton affinity ($\Delta pK_a > 0$), or both. The three cases are schematically illustrated in Scheme 2. Since the observed behavior is similar to pattern b in Scheme 2, we infer that *both* differences in pK_a and a higher intrinsic reactivity should contribute to the higher effective reactivity of the 4-TMPyP species. In the following, we report detailed electronic structure calculations that strongly support this view.

The calculated ground-state total energy differences between the various 2-TMPyP and 4-TMPyP (1–3) species in their S ground state (see below) are used here to provide an estimate of pK_{a1} and pK_{a2} . By approximating the free-energy differences among the various species with the corresponding total-energy differences, calculated for the fully relaxed models, we have an approximation of pK_{a1} and pK_{a2} . The estimate is clearly rather crude because we neglect both

(29) (a) Pasquarello, A.; Laasonen, K.; Car, R.; Lee, C.; Vanderbilt, D. *Phys. Rev. Lett.* **1992**, *69*, 1982. (b) Pasquarello, A.; Laasonen, K.; Car, R.; Lee, C.; Vanderbilt, D. *Phys. Rev. B* **1993**, *47*, 10142.

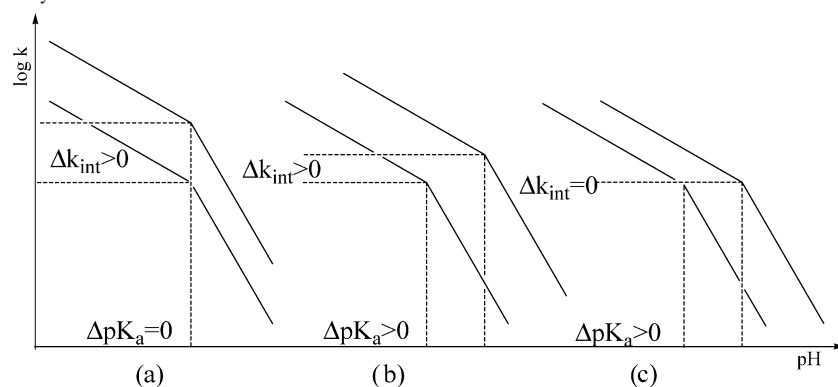
(30) Vanderbilt, D. *Phys. Rev. B* **1990**, *41*, 7892.

(31) Makov, G.; Payne, M. C. *Phys. Rev. B* **1995**, *51*, 4014.

(32) Perdew, J. P.; Chevary, J. A.; Vosko, S. H.; Jackson, K. A.; Pederson, M. R.; Singh, D. J.; Fiolhais, C. *Phys. Rev. B* **1992**, *46*, 6671.

(33) Perdew, J. P.; Zunger, A. *Phys. Rev. B* **1981**, *23*, 5048.

(34) We note that the inverse reactivity profile we see was not observed for oxo-Mn(V) porphyrins generated photochemically in nonaqueous media where there may be no oxo–hydroxo–aqua equilibrium, see: Zhang, R.; Horner, J. H.; Newcomb, M. *J. Am. Chem. Soc.* **2005**, *127*, 6573–6582.

Scheme 2. Possible Reactivity Patterns^a


^a **a** and **c** correspond to limit situations [$\Delta k_{\text{int}} > 0, \Delta pK_a = 0$] and [$\Delta k_{\text{int}} = 0, \Delta pK_a > 0$], respectively. **(b)** Intermediate regime corresponding to the experimental data [$\Delta k_{\text{int}} > 0, \Delta pK_a > 0$].

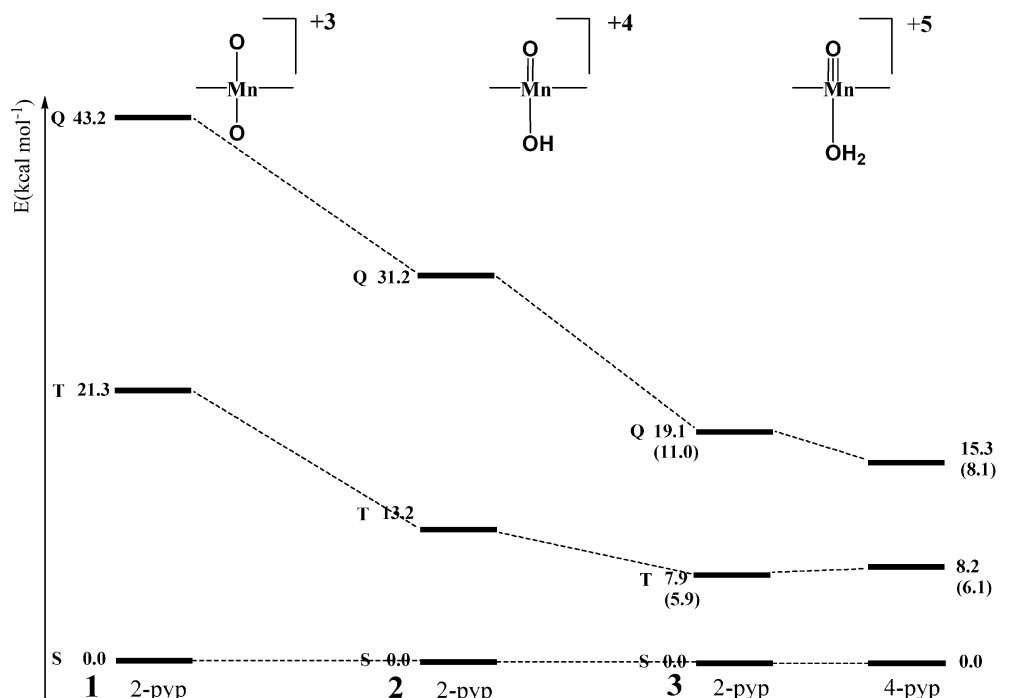


Figure 3. Schematic representation of the energy ordering (kcal mol^{-1}) of the S, T, and Q spin states for species **1**, **2**, and **3** of oxo-Mn(V)-2-TMPyP. For the oxo-Mn(V)-4-TMPyP isomer, only species **3** is reported. For species **3**, data in parentheses correspond to the models including 4 water molecules binding the axial ligands. All energy values have been rescaled so that the S state of every species corresponds to 0.

temperature and solvation effects. However, we expect some error cancellation in the quantity $\Delta[(\Delta pK_a)^{2-4}] = \{[(\Delta pK_{a1})^{2-4}] - [(\Delta pK_{a2})^{2-4}]\}$, which is the difference of the differences $[(\Delta pK_{a2})^{2-4}] = (pK_{a2})^{2\text{-TMPyP}} - (pK_{a2})^{4\text{-TMPyP}}$, and $[(\Delta pK_{a1})^{2-4}] = (pK_{a1})^{2\text{-TMPyP}} - (pK_{a1})^{4\text{-TMPyP}}$. In particular, $[(\Delta pK_{a1})^{2-4}]$ and $[(\Delta pK_{a2})^{2-4}]$ are calculated to be 7.9 and 8.1; as expected, the $[(\Delta pK_{a2})^{2-4}]$ value is considerably overestimated compared to the experimental value (1.1). Nevertheless, our calculations tell us that $[(\Delta pK_{a1})^{2-4}]$ should be similar to $[(\Delta pK_{a2})^{2-4}]$ (i.e., $\Delta[(\Delta pK_a)^{2-4}]$ should be close to zero). This implies that the lines that represent the variation of $\log k$ with pH for the 2-TMPyP and 4-TMPyP isomers should remain approximately parallel at low pH until saturation occurs (i.e., when the only species present in solution is species **3**). This theoretical prediction is in good agreement with the experimental data in the available pH range (Figure 2).

Electronic Structure. We find that the oxo-Mn(V)-2-TMPyP species has a S ground state in all three complexes of interest. The T and Q spin states have higher energies, which depend on the degree of protonation of the axial ligand, as shown in Figure 3. Our results agree with the experimental NMR spectrum of the 2-TMPyP species recorded at pD 8.7 in D_2O ²⁶ and with previous DFT calculations by Ghosh²⁴ on similar oxo-Mn(V) porphyrins using the same XC functional adopted in this study. We find that the diaqua-Mn(III) product of the 2-TMPyP species has a Q ground state, with the T and S states lying 17.1 and 29.3 kcal mol^{-1} above the Q state, respectively; this is also in agreement with available experimental data.³⁵

(35) (a) Goldberg, D. P.; Telsler, J.; Krzystek, J.; Montalban, A. G.; Brunel, L. C.; Barrett, A. G. M.; Hoffman, B. M. *J. Am. Chem. Soc.* **1997**, *119*, 8722. (b) Krzystek, J.; Telsler, J.; Pardi, L. A.; Goldberg, D. P.; Hoffman, B. M.; Brunel, L. C. *Inorg. Chem.* **1999**, *38*, 6121.

Contrasting results from theoretical calculations have been reported in the literature for the ground spin state of oxo-Mn(V) species. In particular, Shaik reported a high-spin ground state for a model oxo-aqua-Mn(V)-porphyrin species,¹⁵ using the hybrid B3LYP XC functional.³⁶ A Mn(V) triplet ground state has also been reported by Siegbahn for an oxo-Mn(V)-tetrahydroxo model complex at the B3LYP level of DFT.³⁷ Although hybrid functionals are usually superior to simple GGA functionals, compared to the latter, they tend to over-stabilize high spin configurations.³⁸ This appears to be the case for the molecules that we study here, which have a S ground state as determined by experiment.²⁶ An excessive bias of hybrid functionals in favor of high-spin configurations was recently found in the case of oxo-Mn(V) salen complexes, which are similar to the presently studied oxo-Mn(V) porphyrins. B3LYP predicts a triplet ground state for the oxo-Mn(V) salen complexes,^{39,40} while both GGA and CCSD(T) calculations predict a singlet ground-state.^{41,42} We note that experimental evidence indicates a singlet ground state for an oxo-Mn(V) salen complex on the basis of the similarity of the NMR spectrum with that of the corresponding nitrido-Mn(V) salen species.⁴³

The relative energies of the S, T, and Q spin states in complexes **1**, **2**, and **3** are reported in Figure 3. As can be seen, the S–T and the S–Q gaps decrease if the degree of protonation of the axial ligand of the 2-TMPyP isomer increases. Species **3** has the smallest S–T and S–Q gaps (7.9 and 19.1 kcal mol⁻¹, respectively). This reflects a change in the electronic structure caused by the replacement of one oxo-axial ligand in the dioxo compound **1** with hydroxo and aqua groups in **2** and **3**, respectively. The net effect is a reduction of the trans effect on the residual oxo group and of the σ – π donation to the metal. The stabilization of higher spin states with protonation of the axial ligands suggests that the observed activation at low pH could be related to T and Q spin states that become accessible and are in turn associated with a weakening of the oxo–Mn bond. Indeed, for the S state of species **3**, we compute a formal triple oxygen–manganese bond of 1.56 Å for both the 2-TMPyP and 4-TMPyP isomers, in excellent agreement with experimental values in the range of 1.55–1.56 Å⁴⁴ and with previous theoretical calculations.²⁴ We find that the oxo–

Table 1. Electronic Configuration and Mn–O Distance (Å) for the S, T, and Q Spin States of the Oxo-aqua-Mn(V)-TM-2-pyridyl Porphyrin Species **3**

electronic configuration	r_{MnO}
S [$d_{xy}(2)$, $A_{2u}(2)$, $A_{1u}(2)$, $d_{\pi-\pi^*}(0)$, $d_{\pi-\pi^*}(0)$]	1.56
T [$d_{xy}(1)$, $A_{2u}(2)$, $A_{1u}(2)$, $d_{\pi-\pi^*}(1)$, $d_{\pi-\pi^*}(0)$]	1.64
Q [$d_{xy}(1)$, $A_{2u}(1)$, $A_{1u}(2)$, $d_{\pi-\pi^*}(1)$, $d_{\pi-\pi^*}(1)$]	1.73

Mn bond length increases to 1.64 and 1.73 Å, respectively, in the T and Q spin configurations, as shown in Table 1. Ultimately, oxo-Mn(V) Q spin states are better described as oxyl-Mn(IV) electronic states, with a single oxygen–manganese bond and ca. one unpaired electron localized on the oxygen atom. Notably, a low-lying oxyl-Mn(IV) electronic state has been proposed to be a key requisite for models of the photosynthetic water oxidizing complex.³⁷ We also notice that the inclusion of 4 water molecules bound to the axial ligands in species **3** does not lead to a change in the spin-state ordering, even though a general stabilization of the T and Q states with respect to the S state is calculated (see Figure 3). This stabilization of higher-spin multiplicities upon partial inclusion of solvation is caused by the increased electron density available on the oxo ligand in the T and Q spin states with respect to the S ground state, see below.

We now analyze in detail our results on the electronic structure of the 2-TMPyP and 4-TMPyP isomers of the reactive species **3**. In Figure 4, we report isodensity surface plots of the highest-occupied and lowest-unoccupied molecular orbitals belonging to the S ground state of the 2-TMPyP isomer in species **3**. The HOMO-2 orbital, having metal d_{xy} character, is followed, in order of increasing energy, by the porphyrin A_{2u} (HOMO-1) and A_{1u} (HOMO) orbitals. The LUMO consists of a pair of degenerate orbitals with $d_{\pi-\pi^*}$ character made by antibonding combinations of metal d_{xz} – d_{yz} and oxygen p_x – p_y orbitals. This electronic structure for the S ground state is in agreement with previous calculations.¹⁵ In the T state, the d_{xy} orbital and one orbital of the $d_{\pi-\pi^*}$ pair are singly occupied while the Q state is formally obtained from the T state by promoting one of the two electrons in the A_{2u} orbital to the remaining empty orbital of the $d_{\pi-\pi^*}$ pair, as can be deduced from the electronic configurations reported in Table 1. The fact that in the T state the d_{xy} orbital is singly occupied, rather than the higher-lying A_{2u} orbital in the starting S configuration, is the result of the strong exchange interaction between the metal orbitals. This picture of the electronic structure correlates well with the elongation of the oxo–Mn bond in the T and Q states, also reported in Table 1, which reflects single and double occupancy of the antibonding $d_{\pi-\pi^*}$ pair.

Interestingly, Figure 3 shows that while the S–T gap is almost the same in the 2-TMPyP and the 4-TMPyP isomers of species **3**, the Q state of the 4-TMPyP isomer is 3.8 kcal mol⁻¹ lower than the corresponding state in the 2-TMPyP isomer (2.9 kcal mol⁻¹, when considering the system

- (36) Becke, A. D. *J. Chem. Phys.* **1993**, *98*, 5648.
 (37) Siegbahn, P. E. M.; Crabtree R. H. *J. Am. Chem. Soc.* **1999**, *121*, 117.
 (38) (a) Rehier, M.; Salomon, O.; Hess, B. A. *Theor. Chem. Acc.* **2001**, *107*, 48. (b) Reiher, M.; Hess, B. A. *Chem.—Eur. J.* **2002**, *8*, 5332.
 (39) Linde, C.; Akermark, B.; Norrby, P. O.; Svensson, M. *J. Am. Chem. Soc.* **1999**, *121*, 5083.
 (40) (a) Khavrutskii, I. V.; Musaev, D. G.; Morokuma, K. *Inorg. Chem.* **2003**, *42*, 2606. (b) Khavrutskii, I. V.; Musaev, D. G.; Morokuma, K. *J. Am. Chem. Soc.* **2003**, *125*, 13879. (c) Khavrutskii, I. V.; Rahim, R. R.; Musaev, D. G.; Morokuma, K. *J. Phys. Chem. B* **2004**, *108*, 3845.
 (41) (a) Cavallo, L.; Jacobsen, H. *Angew. Chem., Int. Ed.* **2000**, *39*, 589. (b) Cavallo, L.; Jacobsen, H. *Inorg. Chem.* **2004**, *43*, 2175. (c) Jacobsen, H.; Cavallo, L. *Phys. Chem. Chem. Phys.* **2004**, *6*, 3747.
 (42) (a) Abashkin, Y. G.; Collins, J. R.; Burt, S. K. *Inorg. Chem.* **2001**, *40*, 4040. (b) Abashkin, Y. G.; Burt, S. K. *J. Phys. Chem. B* **2004**, *108*, 2708. (c) Abashkin, Y. G.; Burt, S. K. *Chem. Lett.* **2004**, *6*, 59–62. (d) Abashkin, Y. G.; Burt, S. K. *Inorg. Chem.* **2005**, *40*, 1425.
 (43) Bryliakov, K. P.; Babushkin, D. E.; Talsi, E. P. *J. Mol. Catal. A* **2000**, *158*, 19.

- (44) (a) Collins, T. J.; Gordon-Wylie, S. W. *J. Am. Chem. Soc.* **1989**, *111*, 4511. (b) Collins, T. J.; Powell, R. D.; Slobodnick, C.; Uffelman, E. S. *J. Am. Chem. Soc.* **1990**, *112*, 899. (c) MacDonnell, F. M.; Fackler, N. L. P.; Stern, C.; O'Halloran, T. V. *J. Am. Chem. Soc.* **1994**, *116*, 7431.

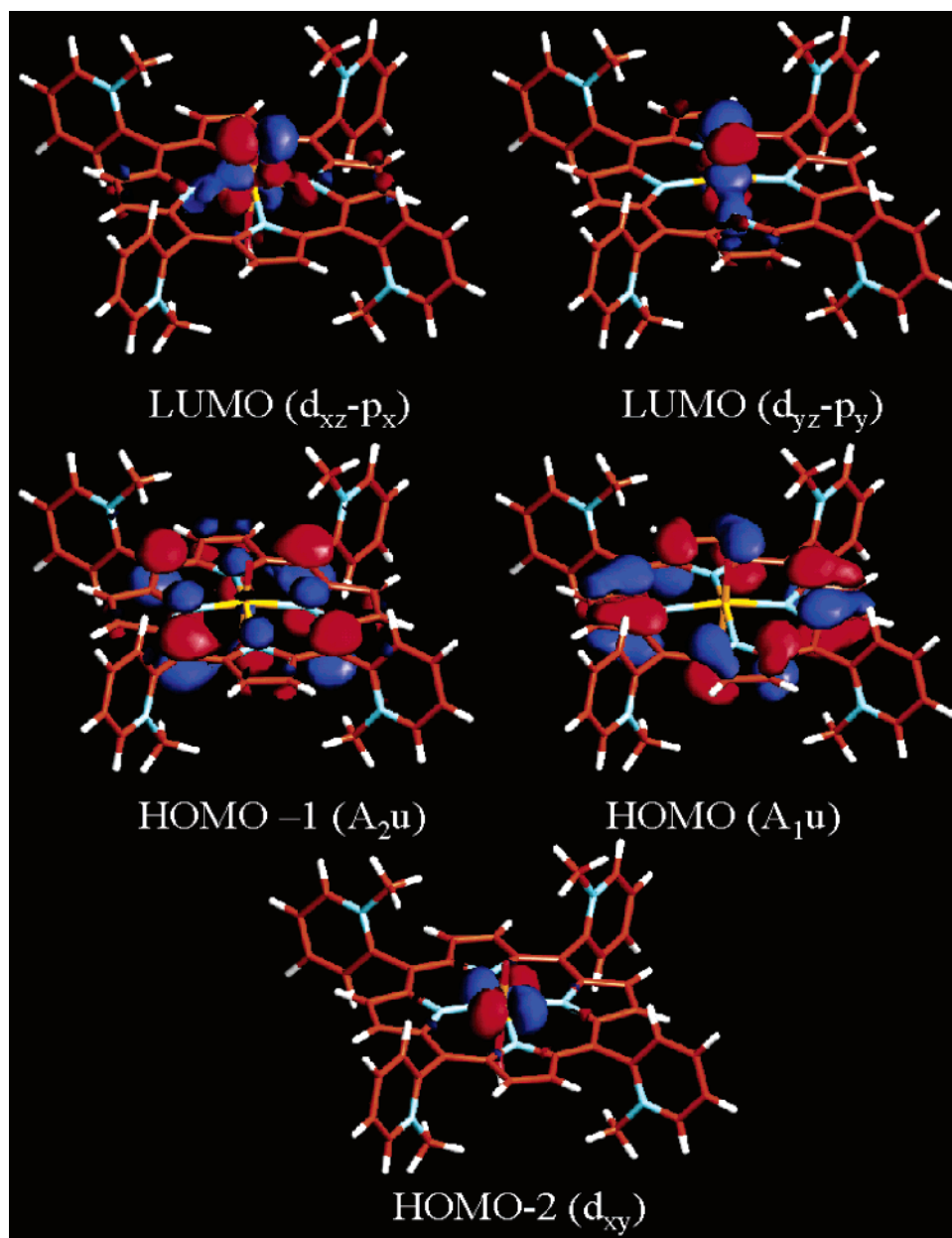


Figure 4. Relevant frontier molecular orbitals for the S state of the oxo-aqua-Mn(V)-2-TMPyP (**3**).

including 4 water molecules). This effect can be understood by looking at the orbital energy level diagram in Figure 5. The orbital energies of the HOMO–2, HOMO–1, HOMO, and LUMO of the 2-TMPyP and 4-TMPyP isomers in the S ground state of species **3** are reported in this diagram. To facilitate the comparison, the d_{xy} levels of the two isomers have been aligned; notice, however, that the d_{xy} orbital of 2-TMPyP species **3** is stabilized by 0.40 eV with respect to that of 4-TMPyP, suggesting that in the 2-TMPyP species the metal center experiences a decreased electron donation from the porphyrin ligand than in 4-TMPyP.

As is evident from Figure 5, the $d_{xy}/d_{\pi}-\pi^*$ separation is essentially the same in the two isomers (1.08 and 1.09 eV in 2-TMPyP and 4-TMPyP, respectively), but the order of the A_{1u} and A_{2u} levels is reversed in the two isomers. In particular, the A_{2u} level becomes the HOMO in the 4-TMPyP isomer. This effect originates from the stronger electron-

withdrawing character of the 2-pyridyl meso substituents compared to the isomeric 4-pyridyl, which stabilizes the A_{2u} level in the 2-TMPyP case. The A_{2u} orbital has large coefficients on both the porphyrin nitrogens and the meso carbons that link to the 2-pyridyl and 4-pyridyl substituents. Thus, one expects the A_{2u} orbital to be more sensitive to changes in the meso substituents than the A_{1u} orbital, which has a node on the meso carbons, as one can see in Figure 4. As a consequence, while the d_{xy}/A_{1u} separation is essentially unaffected by changing the meso-substituents (0.52 and 0.53 eV in 2-TMPyP and 4-TMPyP, respectively), the $A_{2u}/d_{\pi}-\pi^*$ separation decreases from 0.60 eV in 2-TMPyP to 0.46 eV in 4-TMPyP. On the other hand, as already discussed above, the $d_{xy}/d_{\pi}-\pi^*$ separation is not significantly affected by the meso substituents. These findings explain why an S–T excitation, in which a d_{xy} electron is promoted to the $d_{\pi}-\pi^*$ pair, has essentially the same cost in the 2-TMPyP and the

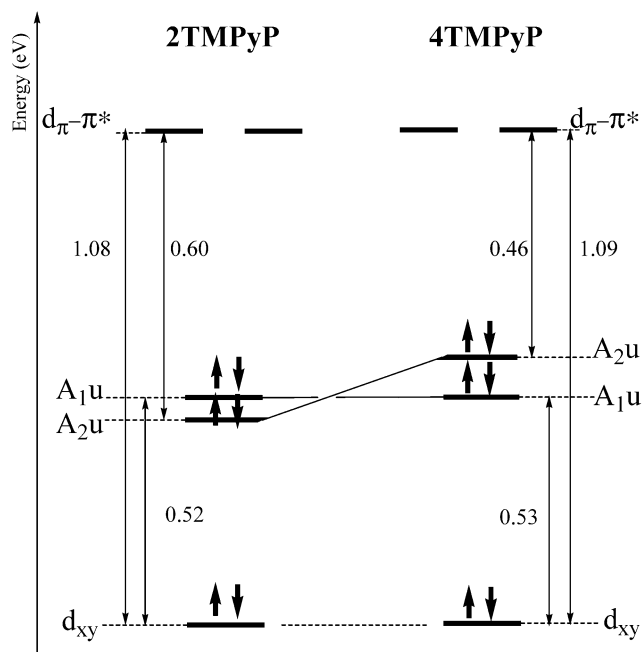


Figure 5. Molecular orbital energy differences (eV) for the S states of the oxo-aqua-Mn(V)-2-TMPyP and oxo-aqua-Mn(V)-4-TMPyP porphyrins **3**. The energy levels of the d_{xy} orbitals have been aligned to zero.

4-TMPyP isomers, resulting in an almost identical S–T gap in the two isomeric porphyrins. A S–Q excitation, on the other hand, has a smaller cost in the 4-TMPyP isomer than in the 2-TMPyP isomer because, in the former, such excitation requires promoting an additional electron from the destabilized A_{2u} level to the remaining empty $d_{\pi-\pi^*}$ level. This accounts for the reduced S–Q and T–Q gaps computed for the 4-TMPyP isomer.

We note that the T and Q spin states are natural precursors to the breaking of the oxo–Mn bond, which gets progressively weakened when the spin state changes from S to T and then from T to Q (Table 1). Since the final product of the reaction is a Mn(III) diaqua species, which has a Q ground state, at some point along the reaction coordinate the S potential energy surface of the reactants has to cross the Q potential energy surface of the products,⁴⁵ possibly with the intermediacy of the T spin surface.

Reactivity. To check the effect of the particular spin state on the reactivity of oxo-Mn(V) porphyrins with Br^- , we performed additional calculations considering a simplified model of the oxo-aqua-Mn(V) porphyrin **3**, in which the meso substituents were replaced by hydrogen atoms (Figure 6). In particular, we optimized the geometry of the Br^- adduct with the oxo-aqua-Mn(V)-porphyrin model considering the three different S, T, and Q spin states, and we included an additional water molecule in our model, which should eventually replace the outgoing BrO^- product in the coordination sphere of the metal center. The resulting structures are reported in Figure 6, in which the main geometrical parameters for the three spin states and their relative energies have been reported. In Table 2, atomic

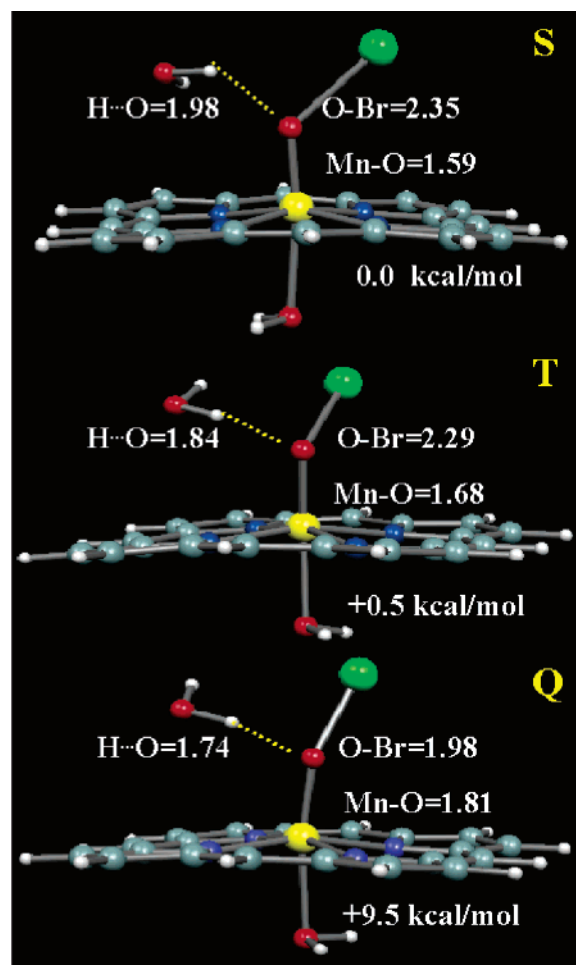


Figure 6. Optimized molecular structures of the S, T, and Q spin states of the Br^- -oxo-aqua-Mn(V)-porphyrin adducts. Main bond lengths (Å) are reported, as well as energies relative to that of the S ground state (kcal mol^{-1}).

Table 2. Charges (q) and Atomic Spin Densities (ρ) for the S, T, and Q Spin States of the Br^- -oxo-Mn(V)-porphyrin Adducts at Their Equilibrium Geometries

spin state	Mn		O		Br	
	q	ρ	q	ρ	q	ρ
S	1.29	0.00	-0.26	0.00	-0.35	0.00
T	1.30	2.29	-0.34	0.10	-0.26	0.30
Q	1.24	2.94	-0.43	0.50	-0.13	0.57

charges and atomic spin densities on the Mn, O (oxo), and Br atoms have been reported.

For the Br^- -oxo-aqua-Mn(V)-porphyrin adducts, we find a S ground state followed in order of increasing energy by the T and Q states, lying respectively 0.5 and 9.5 kcal mol^{-1} above the S state. We therefore see that even though the order of the spin states is qualitatively the same as that for the isolated 2-TMPyP and 4-TMPyP species, the S and T states are now almost degenerate, with the Q state being stabilized with respect to the isolated porphyrins. We note that this effect is the result of the interaction with Br^- and not of the simplification in the porphyrin ligands, since for the oxo-Mn(V)-porphyrin model, we compute an S ground state, with T and Q states lying 9.0 and 16.1 kcal mol^{-1} higher in energy, respectively, similar values to those found for the oxo-aqua-Mn(V) 2-TMPyP and 4-TMPyP species.

(45) (a) Shaik, S.; Filatov, M.; Schröder, D.; Schwartz, H. *Chem.—Eur. J.* **1998**, *4*, 193. (b) Filatov, M.; Shaik, S. *J. Phys. Chem.* **1998**, *102*, 3835.

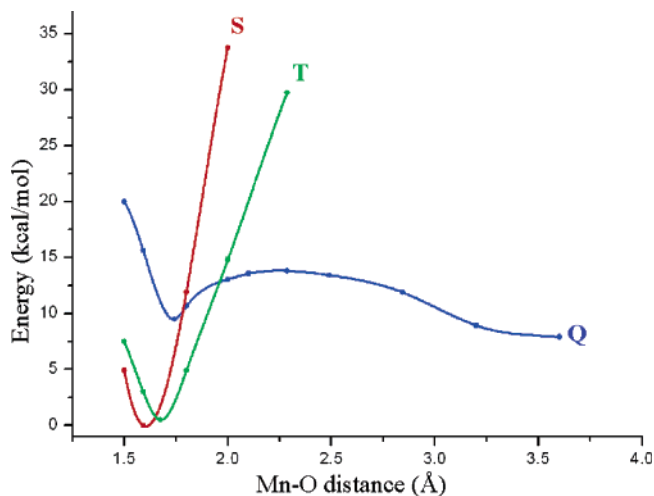


Figure 7. Potential energy profiles (kcal mol⁻¹) for the S (red), T (green), and Q (blue) spin states of the Br⁻-oxo-aqua-Mn(V)-porphyrin adducts as a function of the Mn-O bond length. The calculated points (shown as filled circles) have been interpolated by spline functions.

Inspection of the geometrical structures of the Br⁻-oxo-aqua-Mn(V)-porphyrin adducts in their S, T, and Q spin states (Figure 6) reveals that the interaction with Br⁻ substantially increases in the order S < T < Q, as reflected by the shortening of the oxo-Br⁻ bond length from 2.35 Å in the S state to 1.98 Å in the Q state. This increased interaction is accompanied by a lengthening of the oxo-Mn bond from 1.59 Å in the S state to 1.81 Å in the Q state, reflecting the double occupancy of d_π-π* orbitals, as already outlined above for the isolated porphyrins. At the same time, a progressively stronger hydrogen bond with the external water molecule is experienced by the oxo ligand, with the H-O (oxo) distances decreasing from 1.98 to 1.74 Å going from the S to the Q spin state.

These geometrical changes reveal that a progressive charge transfer takes place from Br⁻ to the oxo ligand on going from the S to the Q spin state, as reflected by the increase in the atomic charge on the oxo ligand from -0.26 to -0.43 and from the decrease of the Br atom charge from -0.35 to -0.13 upon going from the S to the Q spin state (see Table 2). The increased charge transfer observed in the Q state is accompanied by an overall spin population on the Mn atom of ca. 3 electrons, suggesting a Mn(IV) formal oxidation state. These data confirm that the oxyl-Mn(IV) electron configuration realized in the Q spin state is the more reactive toward Br⁻.

We then investigated the energy variation of the S, T, and Q spin states of the Br⁻-oxo-aqua-Mn(V)-porphyrin adducts along the approximate reaction coordinate represented by the oxo-Mn bond length. Starting from the optimized structures of the Br⁻-oxo-aqua-Mn(V)-porphyrin adducts in the three possible spin states, we performed a linear transit scan of the potential energy surface along the selected parameter, allowing all the residual degrees of freedom to fully relax. The calculated energy profiles are reported in Figure 7. As can be seen, a sharp increase in the total energy occurs on the S spin surface upon elongation of the oxo-Mn bond. A similar behavior is seen for the T spin surface, although with a reduced curvature of the potential energy surface. A much

softer behavior is observed, on the other hand, for the Q spin surface, which becomes the ground spin-state energy surface for large values of the oxo-Mn bond distance. Indeed, approximate crossings from the S and T to Q spin surfaces are computed to take place for values of the oxo-Mn bond distance of ca. 1.8 and 2.0 Å, respectively. The Q spin surface is favored for long values of the oxo-Mn bond because of the double occupancy of the oxygen-manganese antibonding d_π-π* orbitals, which are lowered in energy as the oxo-Mn bond is stretched. The S-Q and T-Q crossings are approximately located 10.3 and 12.9 kcal mol⁻¹ above the S state equilibrium geometry energy. We also compute a S-T approximate crossing for a value of the oxo-Mn bond of ca. 1.6 Å, lying only 0.8 kcal mol⁻¹ above the S state equilibrium geometry energy.

Most notably, while on the S and T spin surfaces, the energy keeps increasing with increasing values of the oxo-Mn bond, on the Q spin surface a weak barrier lying 4.4 kcal mol⁻¹ above the Q state equilibrium geometry energy (13.9 kcal mol⁻¹ above the S reference state) is computed for a value of the oxo-Mn bond of ca. 2.3 Å. A similar ordering of spin states and reaction profile have been found recently for the dismutation reaction of hydrogen peroxide by an oxo-Mn(V)-salen complex.^{42b-d} Inspection of the geometrical changes occurring along the selected reaction coordinate on the Q spin surface (Figure 8) reveals that coordination of the outer sphere water molecule begins to take place upon elongation of the oxo-Mn bond. At the same time, formation of a BrO⁻ molecule takes place. For values of the oxo-Mn bond larger than 2.8 Å, coordination of the water molecule is completed, thus leading to a Mn(III) diaqua complex and the BrO⁻ product. Figure 8 depicts a series of configurations encountered along the scan of the Q spin surface.

From the data above, we can conclude that once the Br⁻-oxo-aqua-Mn(V)-porphyrin encounter complex has been formed in its S ground state, the largest barrier to the formation of the products is associated with the S-Q crossing. Thus, it is this spin-state crossing that is occurring in the rate-determining step. Assuming that the shapes of the potential energy surfaces for each spin state and the crossing probabilities do not change between the two isomeric porphyrins, if the same difference in the S-Q separation calculated for the isolated 2-TMPyP and 4-TMPyP isomers at their equilibrium geometries (3.8 kcal mol⁻¹) is maintained throughout the reaction profile, we would compute a higher S-Q crossing for the 2-TMPyP than for the 4-TMPyP system, thus explaining the intrinsic difference in the reactivity of the two isomeric porphyrins. Similar arguments would explain the higher reactivity of the 4-TMPyP system, even if the system would initially cross from the S to the T spin surface and then to the Q spin surface, since we compute a 4.1 kcal mol⁻¹ difference in the T-Q gaps for the two isomeric porphyrins at their equilibrium geometries. Finally, we note that the difference in the S-Q and S-T gaps calculated for the 2-TMPyP and 4-TMPyP systems closely compares with the experimental

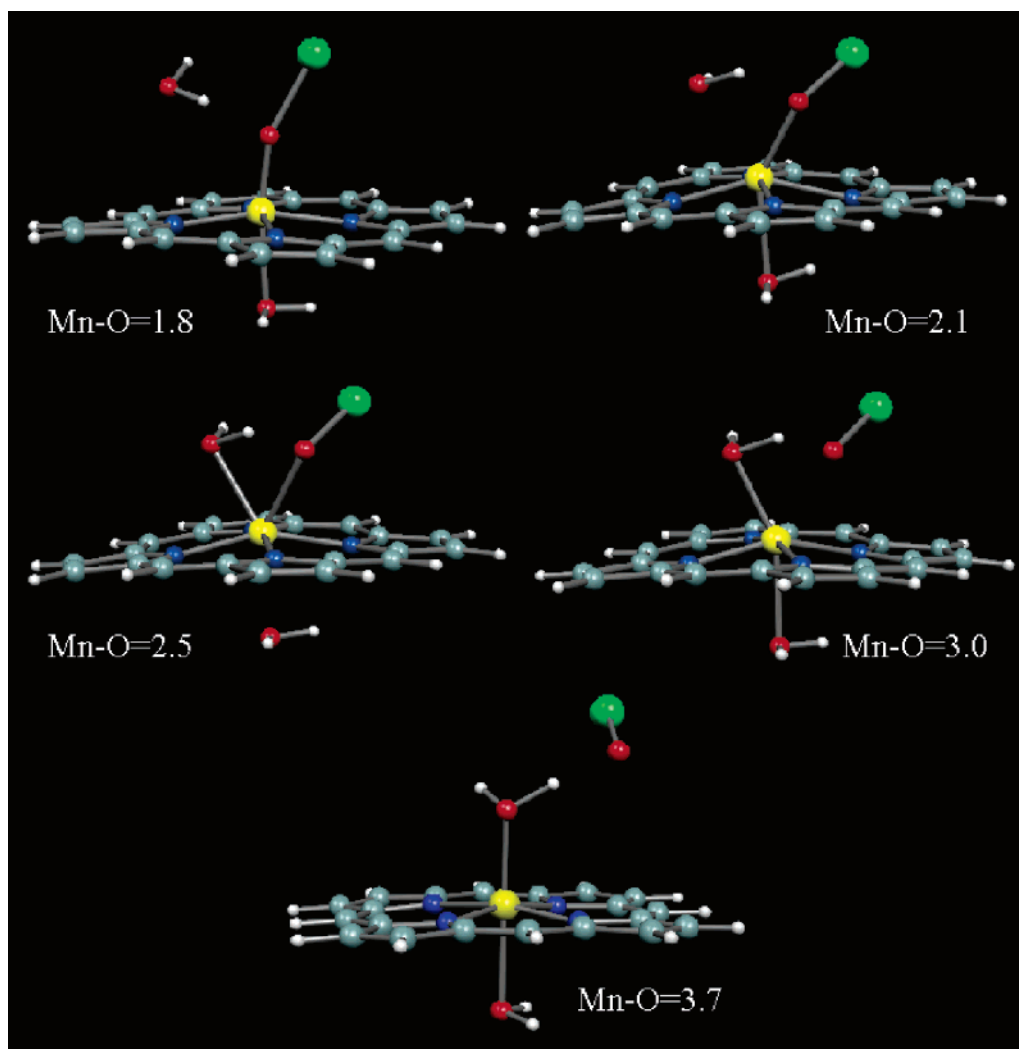


Figure 8. Optimized molecular structures on the Q potential energy surface for the approach of the bromide ion to oxo-Mn(V)-porphyrin as a function of the Mn–O (oxo) bond length (Å).

difference in the activation energies of ca. 3 kcal mol⁻¹ measured for the two isomeric porphyrins.

Conclusions

The reactivity of the isomeric oxo-Mn(V)-tetra-*N*-methyl-2-pyridyl (2-TMPyP) and oxo-Mn(V)-tetra-*N*-methyl-4-pyridyl (4-TMPyP) porphyrins has been investigated by a combined experimental and theoretical approach based on density functional theory.

Two factors are found to contribute to the higher reactivity of the more electron-rich 4-TMPyP species. The oxo ligand of the 4-TMPyP isomer is more basic; so at the same pH, a larger fraction of the reactive oxo-aqua species **3** is present for the 4-TMPyP isomer than for the 2-TMPyP isomer. This predicted p*K*_a difference has been confirmed by the experimental results. At the same time, the low-spin–high-spin promotion energy is smaller for the 4-TMPyP isomer than for 2-TMPyP isomer because of the stabilization of the A_{2u} orbital in the latter isomer. Therefore, in a two-state energy profile⁴⁵ involving crossing of the initial singlet and final

quintet potential energy surfaces, the 4-TMPyP isomer is kinetically favored. The calculated difference in the singlet–quintet gaps for the 2-TMPyP and 4-TMPyP systems compares well with the measured difference in the activation energies for two isomeric porphyrins.

In conclusion, both proton affinity and electron promotion energy contribute to reduce the reactivity of the more electrophilic oxo-manganese(V) complex. The overall effect, which is in marked contrast to the usual expectations based on simple chemical reactivity correlations, results from cooperative modulation of the porphyrin HOMO energy levels and axial ligand prototropy that result from the increased electron-withdrawing character of the 2-pyridinium groups at the meso positions of the porphyrin.

Acknowledgment. Support of this research by the National Science Foundation (CHE 0316301 to J.T.G.) and (CHE-021432 to R.C.) is gratefully acknowledged.

IC060306S